Production of $^{3}_{\Lambda}$H and $^{4}_{\Lambda}$H in central 11.5 GeV/c Au+Pt heavy ion collisions

T. A. Armstrong,[8,*] K. N. Barish,[3] S. Batsouli,[13] S. J. Bennett,[12] M. Bertaina,[7,†] A. Chikanian,[13] S. D. Coe,[13,‡] T. M. Cormier,[12] R. Davies,[9,§] C. B. Dover,[1,‖] P. Fachini,[12,¶] B. Fadem,[5] L. E. Finch,[13] N. K. George,[13,**] S. V. Greene,[11] P. Haridas,[7,††] J. C. Hill,[5] A. S. Hirsch,[9] R. Hoversten,[5] H. Z. Huang,[2] H. Jaradat,[12] B. S. Kumar,[13,‡‡] T. Lainis,[10] J. G. Lajoie,[5] R. A. Lewis,[8] Q. Li,[12] B. Libby,[5,§§] R. D. Majka,[13] T. E. Miller,[11] M. G. Munhoz,[12] J. L. Nagle,[4] I. A. Pless,[7] J. K. Pope,[13,‖‖] N. T. Porile,[9] C. A. Pruneau,[12] M. S. Z. Rabin,[6] J. D. Reid,[11,¶¶] A. Rimai,[9,a] A. Rose,[11] F. S. Rotondo,[13,b] J. Sandweiss,[13] R. P. Scharenberg,[9] A. J. Slaughter,[13] G. A. Smith,[8] X. M. L. Tincknell,[9,c] W. S. Toothacker,[8,‖] G. Van Buren,[7,2,¶] F. K. Wohn,[5] and Z. Xu[13]

(E864 Collaboration)

[1]*Brookhaven National Laboratory, Upton, New York 11973, USA*
[2]*University of California at Los Angeles, Los Angeles, California 90095, USA*
[3]*University of California at Riverside, Riverside, California 92521, USA*
[4]*Columbia University, New York 10027, USA*
[5]*Iowa State University, Ames, Iowa 50011, USA*
[6]*University of Massachusetts, Amherst, Massachusetts 01003, USA*
[7]*Massachusetts Institute of Technology, Cambridge, Massachusetts 02139, USA*
[8]*Pennsylvania State University, University Park, Pennsylvania 16802, USA*
[9]*Purdue University, West Lafayette, Indiana 47907, USA*
[10]*United States Military Academy, West Point, New York 10996, USA*
[11]*Vanderbilt University, Nashville, Tennessee 37235, USA*
[12]*Wayne State University, Detroit, Michigan 48201, USA*
[13]*Yale University, New Haven, Connecticut 06520, USA*

(Received 3 October 2003; published 19 August 2004)

We present measurements from BNL AGS Experiment 864 of the $^{3}_{\Lambda}$H yield and of an upper limit on the $^{4}_{\Lambda}$H yield in central 11.5A GeV/c Au+Pt collisions. The measurements span a rapidity range from center of mass, $y_{\mathrm{c.m.}}$, to $y_{\mathrm{c.m.}}+1$ and a transverse momentum range of $0<p_t\leqslant 1.5$ GeV/c. We compare these results with E864 measurements of stable light nuclei and particle unstable nuclei yields of the same baryon number. The implications of these results for the coalescence of strange clusters are discussed.

DOI: 10.1103/PhysRevC.70.024902 PACS number(s): 25.75.−q, 21.80.+a

I. INTRODUCTION

Relativistic heavy-ion collisions are the main experimental tool for studying the behavior of nuclear matter under conditions of extreme energy and baryon density. In addition, these collisions offer the only method to produce large multistrange bound systems in a controlled manner, since they provide copious strangeness production.

Hypernuclei, which are nuclei in which at least one nucleon is replaced by a hyperon, exist and have been studied for many years. More exotic forms of multistrange nuclear systems have been hypothesized to exist. These include MEMOS (metastable exotic multihypernuclear objects) [1] which may be neutral or even negatively charged and strangelets [2–4] which are single "bags" of approximately equal numbers of strange, up and down quarks with baryon number greater than 1. In many cases the quantum numbers of the proposed MEMOS and of strangelets are the same. In these cases, and assuming strangelets exist, the MEMOS would decay into the more deeply bound strangelets. The production of these exotic hypernuclei could then be a doorway to the production of strangelets. In Experiment 864, 10% most central, 11.5 GeV/c per nucleon Au on Pt or Pb collisions were sampled in a search for strangelets with $A<100$ and lifetimes greater than 50 ns. No strangelets were observed at a level of $\approx 10^{-8}$ per central collision [5–7].

The study of the production of the light hypernuclei $^{3}_{\Lambda}$H and $^{4}_{\Lambda}$H is very instructive in understanding the production

*Present address: Vanderbilt University, Nashville, Tennessee 37235.
†Present address: Istituto di Cosmo-Geofisica del CNR, Torino, Italy/INFN Torino, Italy.
‡Present address: Anderson Consulting, Hartford, CT.
§Present address: Univ. of Denver, Denver, CO 80208.
‖Deceased.
¶Present address: Argonne National Laboratory, 9700 S. Cass Ave., Argonne, Illinois 60439.
**Present address: Cambridge Systematics, Cambridge, MA 02139.
††Present address: McKinsey & Co., New York, NY 10022.
‡‡Present address: Department of Radiation Oncology, Medical College of Virginia, Richmond, VA 23298.
§§Present address: University of Tennessee, Knoxville, TN 37996.
‖‖Present address: Geology and Physics Dept., Lock Haven University, Lock Haven, PA 17745.
¶¶Present address: Institut de Physique Nucléaire, 91406 Orsay Cedex, France.
[a]Present address: Institute for Defense Analysis, Alexandria, VA 22311.
[b]Present address: MIT Lincoln Laboratory, Lexington, MA 02420-9185.
[c]Present address: Brookhaven National Laboratory, Upton, New York 11973.

 ©2004 The American Physical Society

mechanism of exotic objects such as multihypernuclei or MEMOS and the strangelets they might decay into. There are various proposed production mechanisms for multihypernuclei and strangelets in heavy-ion collisions, including quark-gluon plasma distillation [8–10], thermal production [12–15], and coalescence mechanisms [1,11]. In coalescence production of normal nuclei, it is known [16] that when a number of nucleons coalesce there is a "penalty factor" for each nucleon that is added to a cluster. In the case of hypernuclei there is also an additional suppression factor due to the different yields of strange baryons as compared with nucleons. On top of this, it is unknown whether there may also be an extra "strangeness penalty factor" if for some reason strange baryons are less likely than nucleons to participate in coalescence.

The study of light nuclei in E864 [16] is informative about the coalescence process of nucleons at freeze-out and the penalty factor involved when adding a nucleon to a cluster. When the invariant yields of light nuclei with $A=1$ to $A=7$ are examined in a small kinematic region near the center-of-mass rapidity and at low p_t ($p_t/A \leqslant 300$ MeV), they show an exponential dependence on baryon number, suggesting a penalty factor of approximately 48 for each nucleon added. However, in order to determine whether there is some extra strangeness penalty factor when hyperons are coalesced, the study of ${}^{3}_{\Lambda}\mathrm{H}$ and ${}^{4}_{\Lambda}\mathrm{H}$ is important.

Finally, the production of ${}^{3}_{\Lambda}\mathrm{H}$ and ${}^{4}_{\Lambda}\mathrm{H}$ in relativistic heavy-ion collisions is a novel measurement and interesting in itself for further understanding the strangeness degree of freedom in hadronic systems. In this paper we present measurements from BNL AGS Experiment 864 of the ${}^{3}_{\Lambda}\mathrm{H}$ invariant multiplicity and of a 90% confidence level upper limit on the ${}^{4}_{\Lambda}\mathrm{H}$ yield.

II. THE E864 SPECTROMETER

Experiment 864 is an open geometry, high data rate spectrometer designed primarily for the search for strange quark matter produced in relativistic Au+Pt collisions. The open geometry allows for a large region of the phase space for produced heavy clusters to be sampled. A beam of Au ions with momentum 11.5 GeV/c per nucleon is incident on a fixed Pt target. The interaction products can be identified by their charge and mass in the tracking system and by their energy and time of flight in the calorimeter. A detailed description of the E864 apparatus is given in Ref. [17]. Diagrams of the plan and elevation views of the apparatus are shown in Fig. 1.

The tracking system consists of two dipole analyzing magnets ($M1$ and $M2$) with vertical fields, three scintillator time of flight hodoscope planes ($H1, H2$, and $H3$), and two straw-tube stations ($S2$ and $S3$). The dipole magnets $M1$ and $M2$ can be set to different field strengths to optimize the acceptance for various particles of interest. The three hodoscope planes measure the time, charge, and spatial position for each charged particle that passes through them. The straw-tube planes provide improved spatial resolution for the charged tracks. The magnetic rigidity, momentum, and mass of the tracked particles can be determined by the position,

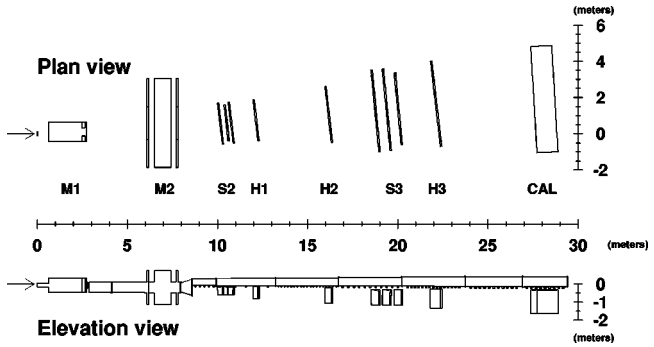

FIG. 1. The E864 spectrometer in plan and elevation views, showing the dipole magnets ($M1$ and $M2$), hodoscopes ($H1$, $H2$, and $H3$), straw tube arrays ($S2$ and $S3$), and hadronic calorimeter (CAL). The vacuum chamber is not shown in the plan view.

time, and charge information from these detectors together with the knowledge of the magnetic field and the assumption that they come from the target. The hadronic calorimeter measures the energy and time of flight for all particles. The calorimeter is the primary detector for identifying neutral particles and can act as a powerful tool for background rejection for charged particles. It has excellent resolution for hadronic showers in energy [$\sigma_E/E = 0.34/(\sqrt{E}) + 0.035$ for E in GeV] and time ($\sigma_t \approx 400$ ps) and is described in detail in Ref. [18]. There is a vacuum tank along the beam line to reduce the background from beam particles interacting downstream. Near the target there are beam counters and a multiplicity counter which are used to set a first level trigger that selects interactions according to their centrality. The calorimeter energy and time of flight measurements are also used to make a level-2 trigger (LET) that rejects interactions which produce no high mass particle in the spectrometer [19]. Each calorimeter phototube amplitude and time are digitized and the digitized results are used to address a lookup table which determines if that time and energy satisfy the trigger. The final LET trigger is just the logical OR of all the phototube lookup table results.

For this study the magnetic field of the spectrometer was −0.2 T, which is the optimum magnetic field for the simultaneous acceptance of both the decay products of the hypernuclei (π^- and ^{3}He or ^{4}He). We triggered on the 10% most central events as defined by our multiplicity counters and used an additional high mass LET trigger which was set for the enhancement of ^{3}He and ^{4}He nuclei. This LET trigger rejected interactions that did not result in any high mass objects in the calorimeter by a factor of approximately 60. In this way, 13.5×10^9 10% most central collisions were sampled as part of this study.

III. DATA ANALYSIS

The light hypernuclei ${}^{3}_{\Lambda}\mathrm{H}$ and ${}^{4}_{\Lambda}\mathrm{H}$ decay weakly via mesonic and nonmesonic channels. Their lifetimes of $\approx 2 \times 10^{-10}$ sec ($c\tau \approx 6$ cm) imply that they decay far outside the collision fireball, so we can observe them through the detection of their decay products which can be identified in the spectrometer [16,17]. Because E864 has good particle iden-

tification for charged particles, we have concentrated on the following mesonic channels.

(1) $^3_\Lambda\mathrm{H} \rightarrow \pi^- + {}^3\mathrm{He}$, branching ratio: 25% [20,21].
(2) $^4_\Lambda\mathrm{H} \rightarrow \pi^- + {}^4\mathrm{He}$, branching ratio: 50% [24,25].

A. $^3_\Lambda$H analysis

The chief problem in reconstructing the $^3_\Lambda$H signal from its decay products is the combinatorial background produced by uncorrelated (^{3}He, π^-) pairs. In order to subtract away this background, the "mixed event method" is used, as explained presently. First, events that contain at least one (^{3}He, π^-) pair are selected. The invariant mass of each such pair is calculated and a histogram of all these invariant masses is created. This "same event" invariant mass spectrum (SE) contains a small $^3_\Lambda$H signal and a large background that is due to particles that are not the decay products of a hypernucleus. The background shape (Bg) is obtained by constructing the invariant mass spectrum of uncorrelated (^{3}He, π^-) pairs that come from different events (but still only using the subsample of events that contain at least one pair of the particles of interest). Specifically, we combine the daughter particle of one type from one event with all daughter particles of the other type from a number of subsequent events. We have to make sure, however, that the mixed event spectrum does not contain pairs of overlapping ^{3}He and π^- tracks, which for some reason could not be found if both tracks were in the same event. This is achieved by requiring that the ^{3}He and π^- are in different sides of the detector horizontally (in the magnetic bend direction), with the sides assigned to give optimum efficiency for simulated decays.

We then simulate the shape of the hypernucleus mass peak by using a GEANT simulation of the decay products of $^3_\Lambda$H passing through the apparatus and reconstructing their invariant mass spectrum (MC). This gives us the shape that we believe the $^3_\Lambda$H signal should have. Finally, we fit a linear combination of the Monte Carlo shape of the signal and the mixed event spectrum to the same event spectrum,

$$\alpha \times (\mathrm{Bg}) + \beta \times (\mathrm{MC}) = \mathrm{SE}. \quad (1)$$

The determination of the parameters α and β allows us to measure the signal either by subtracting the histogram $\alpha \times$(Bg) from SE and then integrating the subtracted spectrum over the region of the expected signal, or simply as the full integration of $\beta \times$(MC).

As a check of this technique, we looked at the proton -π^- invariant mass spectrum from 6.5×10^6 events to observe the similar signal from Λ decays. In Fig. 2 we show the same event and mixed event spectra, the MC signal, and the subtracted spectrum on which we overlay the MC signal. The agreement between the MC shape and the data is good and the fit suggests a signal of 7.25σ above background. We have calculated the Λ invariant multiplicities in several rapidity and transverse momentum bins and they are found to be in good agreement with measurements from AGS Experiments 891 and 877 [22,23]. This gives us added confidence in this mixed event method.

In order to reconstruct the $^3_\Lambda$H signal, we have to identify its decay products. In defining what tracks we will consider

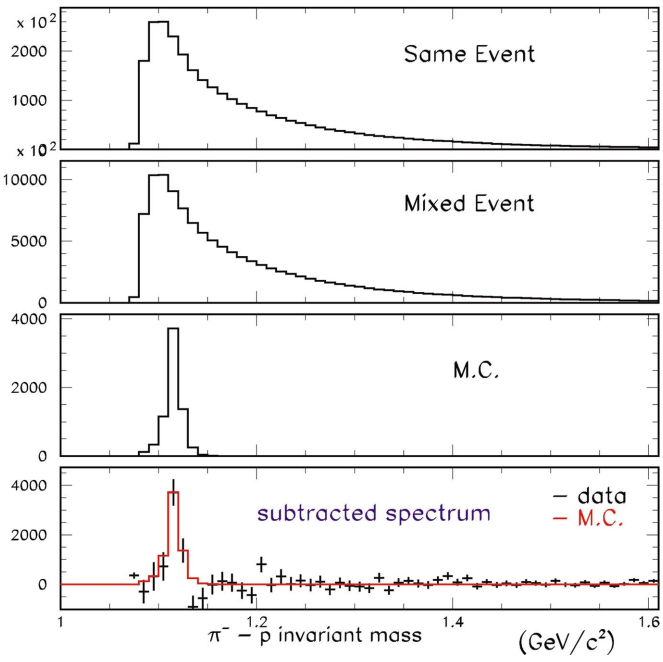

FIG. 2. (Color) The top panel shows the same event invariant mass spectrum for p-π^-. The second panel shows the invariant mass spectrum for p-π^- coming from mixed events. The following panel shows the simulated Λ signal. The bottom panel shows the subtracted invariant mass spectrum for p-π^-, and the solid histogram overlaid on the data is the MC Λ signal.

to be ^{3}He and pions tracks, we generally use very efficient cuts. This is because any background coming from incorrectly identified tracks will be largely subtracted away by the mixed event method (of course, adding extra background does dilute the signal and so at some point opening the cuts further reduces the signal to background ratio). With this in mind, we use the following definitions: A ^{3}He track is defined as a charge two track with rapidity less than 2.7 and reconstructed mass between 1 and 3.4 GeV/c^2. A pion is defined as a negative particle with measured mass less than 0.4 GeV/c^2. Due to the finite time resolution in the hodoscopes, the measured β of a particle could be greater than 1; any such particle with negative charge is defined to be a pion. High efficiency cuts on the quality of tracking fits are also used for both pions and ^{3}He.

When identifying the pion, we avoid imposing strict β or mass cuts which would imply strict time of flight cuts. The reason for this is that both of the decay particles' time of flight measurements have a common start time, so that any fluctuation of the start time will create correlations in the measured masses and velocities of the ^{3}He and π^-. This can then create artificial structure in the same event spectrum which is not present in the mixed event spectrum. Also to avoid creating artificial structure, we divide the apparatus into two horizontal sections and require that the ^{3}He be observed in one part of the detector and the π^- in the other. As noted above, this is to avoid creating mixed events containing overlapping tracks which could not both be found if they were in the same event.

With these definitions for the ^{3}He and pions, we construct the same event invariant mass spectrum (SE) and the mixed-

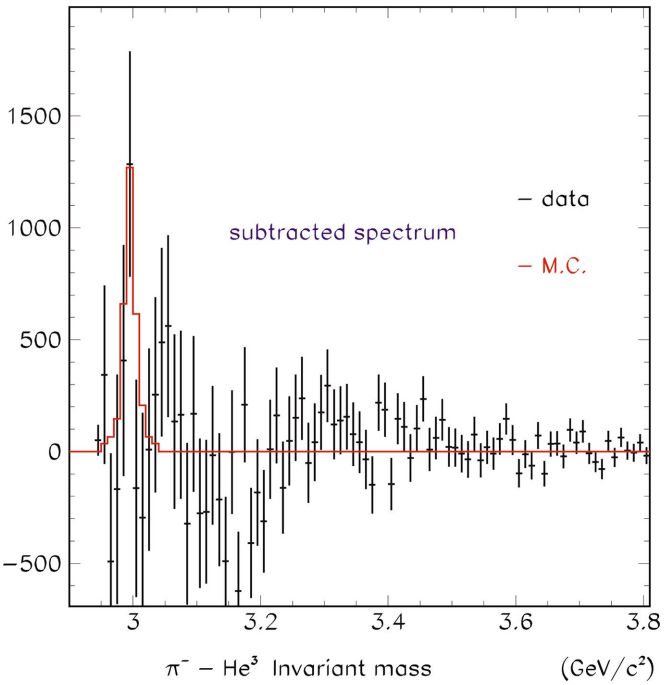

FIG. 3. (Color) Subtracted invariant mass spectrum for ^{3}He-π^- when strict hodoscope cuts are applied on the data. The solid histogram overlaid on the data is the simulated (MC) $^3_\Lambda$H signal normalized so that the peak bin matches the data.

event background spectrum (Bg) as described above (we mix each event with six others in forming the background spectrum). The linear fit, $\alpha\times(\mathrm{Bg})+\beta\times(\mathrm{MC})=\mathrm{SE}$, yields $\beta=3.37\pm1.67$.

This result for the fit parameter β suggests a signal of 2.0 σ. Figure 3 shows the subtracted spectrum $\mathrm{SE}-\alpha\times\mathrm{Bg}$, with the MC shape of the signal overlaid on the data. The χ^2 per d.o.f. of the fit is 1.1 which implies a confidence level of ~32%. If we only perform the linear fit within ten bins of where we expect our signal to be, the signal to background ratio does not change significantly and the confidence level of the fit increases to ~40% which gives us increased confidence that we actually have a signal.

Assuming that the peak in the invariant mass spectrum is a signal, the invariant yield in a rapidity and p_t bin can be calculated. Due to low statistics the yield has to be calculated in a single rapidity ($1.6<y<2.6$) and transverse momentum ($0<p_t<1.5$ GeV/c) bin. This bin includes much of our acceptance, leaving out some of momentum space in which the acceptance changes sharply which would lead to increased systematic errors. Restricting the analysis to this kinematic region does decrease somewhat the significance of the resulting signal.

The invariant multiplicity of the $^3_\Lambda$H is calculated according to

$$Y=\frac{1}{2\pi\overline{p_t}\Delta y\Delta p_t}\times\frac{N_{count}}{N_{sampled}\times\epsilon_{total}\times\eta_{eff}}, \qquad (2)$$

where N_{count} is determined by the linear fit parameters as $N_{count}=\beta\times(\mathrm{MC})$, $N_{sampled}$ is the number of sampled events (13.5×10^9), and Δy, Δp_t, and $\overline{p_t}$ are the momentum bin size and average p_t. ϵ_{total} is the total efficiency for finding a given $^3_\Lambda$H; it includes geometric acceptance, efficiency, of the LET, reconstruction efficiency, method efficiency, and other efficiencies which are listed below. These efficiencies are explained in detail in the following paragraphs.

The geometric acceptance is the fraction of $^3_\Lambda$H nuclei in this kinematic bin whose decay products traverse all the downstream detectors and leave sufficient signals in these detectors. The E864 acceptance is determined by generating a Monte Carlo distribution of $^3_\Lambda$H particles, allowing them to decay into ^{3}He and π^- and tracking the daughter particles using a full GEANT simulation of the experiment. The particle hit information is recorded in each of the detectors and then "faked" by smearing the hits according to the detector resolutions. The faked data is then analyzed in the same manner as the real data but with no cuts besides fiducial cuts. If the $^3_\Lambda$H can be reconstructed from these fake tracks, it is counted as accepted. The geometric acceptance is the ratio of these accepted $^3_\Lambda$H nuclei to the generated ones in the same kinematic bin. For the acceptance calculation, the $^3_\Lambda$H nuclei are generated according to a production model that is Gaussian in rapidity with a width ($\sigma_y=1$) which is determined by folding together the rapidity distribution of the Λ [22,23] and the deuteron [16]. A Boltzmann distribution is assumed for the transverse mass with a temperature (inverse slope) of 450 MeV. In order to study the variation of the acceptance with the assumed production model, different widths of the rapidity distribution (varying from $\sigma_y=0.7$ to 1.1) and slightly different transverse distributions (including a flat distribution in p_t) were used. From these exercises we determined a systematic error of ±9% due to this choice of input distribution.

The LET efficiency is the fraction of the particles of a given species that are selected by using a specific LET lookup table. This trigger efficiency can be calculated by applying the LET lookup table to Monte Carlo simulated showers that the particles of interest create in the calorimeter. For this purpose a Monte Carlo $^3_\Lambda$H distribution is generated and the ^{3}He decay daughters that reach the calorimeter are examined. The peak tower energy and time associated with these ^{3}He nuclei are compared with the actual energy-time lookup table and it is determined whether the tower would or would not fire the trigger. The ratio of the number of Monte Carlo ^{3}H particles that fire the LET to the total number of ^{3}He nuclei that reach the calorimeter is the trigger efficiency. Determining the efficiency by this method has systematic errors that depend on the simulated calorimeter shower response. Also, time shifts (which cannot be fully calibrated away) in the apparatus will cause a difference between the real data and the theoretical lookup table. For these reasons, a more reliable method of calculating the efficiency (especially for low efficiencies like those of $^3_\Lambda$H) is by using the measured numbers of ^{3}He that did and did not fire the trigger. The number of ^{3}He particles firing the trigger is

$$N_{LET}=Y\times N_{evt}\times R\times\epsilon_{LET}. \qquad (3)$$

where Y is the production rate of ^{3}He, N_{evt} the number of LET triggered events, R the trigger rejection factor, and ϵ_{LET}

TABLE I. Efficiencies and invariant yield for $^{3}_{\Lambda}$H in 10% most central Au-Pt collisions in units of c^2/GeV^2 for $1.6<y<2.6$ and $p_t<1.5$ GeV/c.

Rapidity	1.6–2.6
p_t(GeV/c)	0–1.5
N_{event}	13.5×10^9
N_{count}	1220 ± 854
$\epsilon_{total}=\epsilon_{acc}\times\epsilon_{LET}\times\epsilon_{ADDMC}\times\epsilon_{method}$	1.96×10^{-4}
Detector efficiency: η_{det}	0.82^2
Charge cut efficiency: η_q	0.84
Target absorption probability: η_{targ}	0.78
χ^2 cut efficiency: η_{χ^2}	0.90
Invariant yield $(\mathrm{GeV}/c)^{-2}$	$(5.27\pm4.04)\times10^{-4}$

the trigger efficiency. The number of ^{3}He particles not firing the trigger is

$$N_{nonLET}=Y\times N_{evt}\times(1-\epsilon_{LET}), \tag{4}$$

so combining these,

$$\epsilon_{LET}=\frac{N_{LET}}{N_{LET}+R\times N_{nonLET}}. \tag{5}$$

We note that the LET logic is operated on every type of trigger and its output is recorded for every trigger. For "non-LET" triggers the output is simply not used in the trigger decision, thus the LET trigger dead times are the same for all trigger types. Since the LET rejection factor R (and hence the LET efficiency) may vary with varying calibrations, the efficiency is calculated separately for each run and the overall efficiency is the weighted average.

Since it is possible for more than one track to hit the same detector element and for these tracks therefore to not be reconstructed, there is a track reconstruction (or ADDMC) efficiency. The ADDMC efficiency is determined by using Monte Carlo tracks embedded in real events.

The method efficiency is the efficiency of requiring the ^{3}He to be in the left part of the detector and the π^- in the right. It is calculated by counting the number reconstructed (simulated) $^{3}_{\Lambda}$H in a kinematic bin before and after this cut is applied.

The efficiency of the ^{3}He mass cut is calculated using real data to be 97%. A systematic error of 1% is associated with this mass cut, resulting from varying the fit parameters for the mass spectrum. The mass cut for the pions has an efficiency of essentially 100%. Other efficiencies include the charge two cut efficiency, the efficiency of cuts on the χ^2 distributions for various reconstruction fits, and the probability that the $^{3}_{\Lambda}$H will interact with the target. The values of all these efficiencies are listed in Table I. Finally, only $^{3}_{\Lambda}$H that are reconstructed from ^{3}He that fired the LET can be included in our measured signal. The efficiency of this requirement is 84%.

The chief systematic errors which we have identified in this analysis are the 9% systematic error in the calculated acceptance and a 1% systematic error from the fit to the ^{3}He mass peak. The $^{3}_{\Lambda}$H invariant yield, with the statistical and systematic errors combined, is listed in Table I.

Because of the marginal signal, increasing the efficiency in detecting the $^{3}_{\Lambda}$H is important. One way of achieving this is by requiring that ^{3}He and π^- tracks are separated by a specific distance $|\Delta x|$ in the x direction in each of the detector planes instead of requiring that each decay particle is observed in a different side of the detector. However, due to specific considerations that have to be taken into account to ensure that the same and mixed event spectra are treated similarly, we could not in this manner achieve a significantly improved signal to background ratio. The results from this method agree with the results obtained by applying strict hodoscope cuts to within the statistical errors.

As another variation on the analysis, we can instead define the π^- as any negative particle with $p_z<3$ GeV/c (keeping all other cuts the same). We then obtain the fit parameter $\beta=2.79\pm1.69$. The invariant yields obtained from the three different methods agree to within 25% of each other. Though not independent results, the agreement of the results obtained from these various methods makes it more probable that the peak in the invariant mass spectrum is indeed a signal and not just the result of background fluctuations.

B. $^{4}_{\Lambda}$H analysis

The analysis for the $^{4}_{\Lambda}$H is very similar to that for the $^{3}_{\Lambda}$H. The first requirement for the reconstruction of the $^{4}_{\Lambda}$H signal is to identify its decay products, ^{4}He and π^-. A ^{4}He is defined as a charge two object with measured rapidity less than 2.7 and reconstructed mass in the range 3.2–6 GeV/c^2. A pion is defined as a negative charge track with measured β greater than 1.0, or a negative particle with mass less than 0.4 GeV/c^2 (for measured β less than 1.0). It is required that the ^{4}He is observed in the left part of the detector and the π^- in the right part.

With these track requirements, the same event invariant mass spectrum (SE) of is constructed and the background (Bg) shape determined from mixed events (again using six events for mixing). The resulting fit parameter, $\beta=0.8\pm1.4$, suggests that we do not have a statistically significant signal and Fig. 4 shows the subtracted spectrum, $\mathrm{SE}-\alpha\times\mathrm{Bg}$, with the MC shape of the signal overlaid on the data.

To estimate a 90% confidence upper limit of $^{4}_{\Lambda}$H, we choose a reasonable momentum bin $1.8<y<2.6$, $p_t<1.5$ GeV/c. The fit is then performed for events inside this momentum range, and the fit result is $\beta=-0.2\pm1.3$. The fit parameter β is negative which implies that the measured signal ($\beta\times\mathrm{MC}=-53\pm344$) and resultant invariant yield are unphysical due to random error. The way to deal with that is to calculate the invariant yield (Y) and its error δY according to Eq. (2) (even though Y will be unphysical). Then from these numbers we construct the Gaussian with mean Y and variance $(\delta Y)^2$. The physical region of this Gaussian is bounded from below by 0, so our upper limit Y_1 is a number such that the integral from 0 to Y_1 is 90% of the integral from 0 to infinity (all of the physical region) [26].

The various efficiencies involved in this analysis are listed in Table II. Using these and the method described above, the

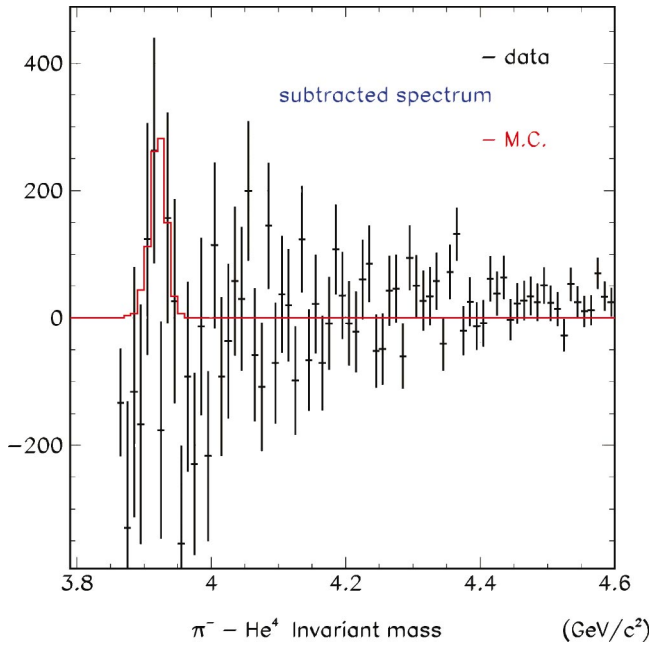

FIG. 4. (Color) Subtracted invariant mass spectrum for ^{4}He-π^- when strict hodoscope cuts are applied on the data. The solid histogram overlaid on the data is the simulated (MC) $^4_\Lambda$H signal.

90% confidence level upper limit for the invariant yield of $^4_\Lambda$H is calculated to be 4×10^{-5} (GeV/c)$^{-2}$.

IV. RESULTS AND DISCUSSION

A. Comparison of hypernuclei production to nonstrange nuclei

E864 has measured the invariant yields of light stable nuclei with mass number $A=1-7$ [16]. It is instructive to compare the yields or limits of these light hypernuclei to the yields of normal nuclei with the same A. Specifically, such a comparison should allow a measurement of the extra penalty factor involved in the coalescence of strangeness, if there is any.

First, we compare the yields of $^3_\Lambda$H and ^{3}He (details of the measurement of ^{3}He can be found in Ref. [16]). The $^3_\Lambda$H yield is approximately a factor of 20 smaller than that of the ^{3}He in the same kinematic region. However, in order to make a statement of whether there is an extra penalty factor when coalescing strangeness, the difference in the production of strange and nonstrange baryons should first be taken into account. Therefore, the relevant quantity is the ratio $Y^3_{\Lambda\mathrm{H}}/Y^3_{\mathrm{He}}\times(Y_\Lambda/Y_p)$, where $Y^3_{\Lambda\mathrm{H}}$, Y^3_{He}, Y_Λ, Y_p are the invariant yields of the particles in the momentum range $1.6<y<2.6$, $p_t<0.5A$ GeV/c. This simple ratio can be misleading, however, since the yields for different species have different kinematic dependences due to collective motion and the efficiency of detecting the $^3_\Lambda$H is strongly momentum dependent. We therefore calculate the following ratio:

$$R=\frac{Y^3_{\Lambda\mathrm{H}}}{\sum_i\left(Y^3_{\mathrm{He}}\times\frac{Y_\Lambda}{Y_p}\times\epsilon\right)_i\Big/\sum_i\epsilon_i}, \tag{6}$$

where the index i runs over the various momentum bins and ϵ_i is the efficiency for detecting the hypernucleus at each bin. To perform the calculation, momentum space is divided into bins of $0.167A$ GeV/c in p_t and 0.2 units in y.

The invariant yields for protons measured by E864 [16] are used to calculate the weighted average yields for each momentum bin. For the kinematic regions where we have not measured protons, we use values obtained by the following parametrization which fits our data:

$$Y\propto m_t\times\exp\left[-\frac{m_t-0.938}{0.212}\right]\times[25.8-0.17(y-y_{\mathrm{c.m.}})^2], \tag{7}$$

where m_t is the transverse mass in units of GeV/c^2. Similarly, for ^{3}He the following parametrization from our data:

$$Y\propto m_t\times\exp\left[-\frac{m_t-2.809}{0.405}\right]\times[8+17(y-y_{\mathrm{c.m.}})^2] \tag{8}$$

is used for the bins where we have no measurement. Finally, for the Λ, results from E891 and E877 were used and the parametrization used [22] is

$$Y\propto\exp\{-m_t[4.3+6.5\cosh(y-y_{\mathrm{c.m.}})-4.2(y-y_{\mathrm{c.m.}})^2]\}. \tag{9}$$

With these numbers we obtain a value of $R=0.36\pm0.26$ for the ratio of Eq. (6). This indicates that there is an extra suppression in the coalescence production of $^3_\Lambda$H of about a factor of 3 compared to that of ^{3}He, after accounting for the different abundances of the coalescence ingredients.

We can then make a similar comparison between $^4_\Lambda$H and ^{4}He, this time using the upper limit we have determined for the $^4_\Lambda$H yield. In E864, the ^{4}He production has been measured [16] and the following parametrization is used for the regions where there is no measurement:

$$Y\propto m_t\times\exp\left[-\frac{m_t-3.727}{0.435}\right]\times[1+3.17(y-y_{\mathrm{c.m.}})^2]. \tag{10}$$

For the $^4_\Lambda$H, we are interested in the ratio

TABLE II. Efficiencies for the $^4_\Lambda$H in 10% most central Au-Pt collisions in units of c^2/GeV^2 for $1.8<y<2.6$ and $p_t<1.5$ GeV/c.

Rapidity	1.8–2.6
p_t(GeV/c)	0–1.5
N_{event}	13.5×10^9
$\epsilon_{total}=\epsilon_{acc}\times\epsilon_{LET}\times\epsilon_{ADDMC}\times\epsilon_{method}$	9.3×10^{-4}
Detector efficiency: η_{det}	0.82^2
Charge cut efficiency: η_q	0.84
Target absorption probability: η_{targ}	0.89
χ^2 cut efficiency: η_{χ^2}	0.90

$$R = \frac{g_R Y_{{}^{4}_{\Lambda}\mathrm{H}}}{\sum_i \left(Y_{{}^{4}\mathrm{He}} \times \frac{Y_\Lambda}{Y_p} \times \epsilon \right)_i \Big/ \sum_i \epsilon_i}, \quad (11)$$

where ϵ_i is the efficiency for detecting the ${}^{4}_{\Lambda}$H and for $Y_{{}^{4}_{\Lambda}\mathrm{H}}$ we use the 90% confidence level upper limit which was determined in Sec. III B.

The factor g_R which appears in the numerator represents a correction due to the fact that ${}^{4}_{\Lambda}$H has a ground state with spin $J=0$ and an excited state with spin $J=1$, while ^{4}He has only a $J=0$ ground state. Because we expect that the invariant yields of different species should be proportional to their spin degeneracy factors $(2J+1)$ [16], we assign $g_R=1/4$. We find then an upper limit from Eq. (11) to be $R<0.225$ at the 90% confidence level. Just as with the ${}^{3}_{\Lambda}$H, this indicates an extra suppression in the production of ${}^{4}_{\Lambda}$H of at least a factor of 4 as compared to that of ^{4}He (after correcting for the differences in abundance of the coalescence ingredients and the spin degeneracies of the different states). What can we conclude from these results?

B. Implications of ${}^{3}_{\Lambda}$H, ${}^{4}_{\Lambda}$H results

There is an apparent suppression in the production of the light hypernuclei as compared with the yields of nonstrange nuclei, which would seem to imply an extra penalty factor for coalescence of strange baryons. However, before drawing such a conclusion, other possible reasons for this suppression should be examined. We will look briefly at two possible explanations.

(1) The relatively large size of these states could be a factor in their production.

(2) Both hypernuclei are very weakly bound and therefore could be easily destroyed in final state soft interactions.

1. Finite size effects

The effect of the finite size of nuclear clusters in their production has been studied by Scheibl and Heinz [27]. Their coalescence model includes the dynamical expansion of the collision zone which results in correlations between the momenta and positions of particles at freeze-out. The invariant spectrum of the formed clusters with mass number A and transverse mass m_t is proportional to some effective volume $V_{eff}(m_t)$, which is approximately proportional to the "homogeneity volume" $[V_{hom}(m_t)]$ of constituent nucleons having transverse mass $m_t=\sqrt{(P_t/A)^2-m_0^2}$. (Here, P_t is the transverse momentum of the nucleus and m_0 is the nucleon mass.) The advantage of using $V_{hom}(m_t)$ is that it is accessible through HBT interferometry measurements.

In this approach, the number of created clusters at a given momentum is calculated by projecting the cluster's density matrix onto the constituent nucleons' density matrices in the fireball at freeze-out. In the case of the deuteron as treated in Ref. [27], one of the internal wave functions considered is the spherical harmonic oscillator with size parameter $d=3.2$ fm. Under various assumptions it is shown that the yield of deuterons is identical with the classic thermal spectrum with only an extra quantum mechanical correction factor, $C_d(R_d,P_d)$, where R_d and P_d are the deuteron's position and momentum space coordinates in the fireball rest frame. C_d provides a measure for the homogeneity of the nucleon phase space around the deuteron center-of-mass coordinates. The measured deuteron momentum spectra do not contain information on the point of formation, so the average correction factor over the freeze-out hypersurface is the relevant quantity, which has a simple approximate form:

$$\langle C_d \rangle \approx \frac{1}{\left[1+\left(\frac{d}{2R_t(m)}\right)^2\right] \times \sqrt{1+\left(\frac{d}{2R_\parallel(m)}\right)^2}}, \quad (12)$$

where $R_\parallel(m_t)$ and $R_t(m_t)$ are the longitudinal and transverse lengths of homogeneity for the constituent nucleons. This implies that the approximate correction factor from thermal production depends only on the ratio of the size parameter of the deuteron's wave function, d, to the radii of homogeneity of the constituent nucleons with zero transverse momentum.

The ${}^{3}_{\Lambda}$H has a rms radius of approximately 5 fm [28], which is much bigger than the rms radius of ^{3}He (1.74 fm). We therefore expect that finite size effects may produce a significant difference in their relative yields. In order to make a rough calculation, we assume that the ${}^{3}_{\Lambda}$H is a system similar to that which consists of a Λ bound to ^{2}H and that the ^{3}He consists of a proton bound to ^{2}H. We further assume a harmonic oscillator internal wave function for the ${}^{3}_{\Lambda}$H with a size parameter equal to the mean distance from the Λ to the center of mass of the ^{2}H, $d({}^{3}_{\Lambda}\mathrm{H})=\sqrt{\langle r^2\rangle_{\Lambda d}}\approx 9.8$ fm (we make the same assumption for ^{3}He, using $d({}^{3}\mathrm{He})=\sqrt{\langle r^2\rangle_{pd}}\approx 2.6$ fm). Under these assumptions, and using a variety of estimates of the radii of homogeneity at the AGS [29–33] (which vary from 3–10 fm), the relevant correction factors can be calculated by using Eq. (12). We find as a rough approximation to the ratio between the two correction factors

$$\frac{C_{{}^{3}_{\Lambda}\mathrm{H}}}{C_{{}^{3}\mathrm{He}}} \approx 0.41 \pm 0.1, \quad (13)$$

which implies that the yield of ${}^{3}_{\Lambda}$H as compared to that of ^{3}He could be a factor between 2 and 3 smaller just due to size effects.

In the case of ${}^{4}_{\Lambda}$H, its rms radius of 2 fm [28] is not much bigger than the ^{4}He radius (1.41 fm). Following a similar treatment as before (with size parameters $d_{{}^{4}_{\Lambda}\mathrm{H}}=\sqrt{\langle r^2\rangle_{\Lambda t}}\approx 3.9$ fm and $d_{{}^{4}\mathrm{He}}=\sqrt{\langle r^2\rangle_{pt}}\approx 1.9$ fm), we have

$$\frac{C_{{}^{4}_{\Lambda}\mathrm{H}}}{C_{{}^{4}\mathrm{He}}} \approx 0.87, \quad (14)$$

so this finite size effect is a relatively small correction in the case of the ${}^{4}_{\Lambda}$H.

2. Small binding energy

E864 has previously reported that the yields of light nuclei near midrapidity and at low p_t are well described by the formula $(1/48)^A \times \exp[-B/T_s]$ where B is the binding energy per nucleon and $T_s=5.9\pm1.1$ MeV [34]. This binding energy

dependence cannot be explained by the coalescence or thermal models that assume a simple exponential dependence on the total binding energy B of the form $\exp[-B/T]$ with the temperature T of the collisions at freeze-out on the order of 100–140 MeV.

The binding energy per nucleon of the ${}^{3}_{\Lambda}\mathrm{H}$ is 0.8 MeV compared to $B=2.7$ MeV for ${}^{3}\mathrm{He}$. Therefore, by taking into account the exponential dependence described above, the ${}^{3}_{\Lambda}\mathrm{H}$ yield should be only 70% of that of ${}^{3}\mathrm{He}$ simply due to the small binding energy. In the case of the ${}^{4}_{\Lambda}\mathrm{H}$ ($B=2.5$ MeV) and the ${}^{4}\mathrm{He}$ ($B=7$ MeV) the effect is even bigger—we would expect suppression by a factor of 2.2 due to the difference in binding energies.

While examining the effect of the binding energy in the production of hypernuclei, it is also instructive to compare the ${}^{4}_{\Lambda}\mathrm{H}$ yield to that of the particle unstable nucleus ${}^{4}\mathrm{H}$, which also has a small binding energy and has been measured (along with other particle-unstable nuclei [35]) by E864. Proceeding as before, we form the ratio

$$R=\frac{g_R Y_{{}^{4}_{\Lambda}\mathrm{H}}}{\sum_i \left(Y_{{}^{4}\mathrm{H}}\times\frac{Y_\Lambda}{Y_n}\times\epsilon\right)_i \Big/ \sum_i \epsilon_i}. \tag{15}$$

g_R is $12/4$ in this case because ${}^{4}\mathrm{H}$ has a $J=2$ ground state and three excited $(J=1,0,1)$ states, giving a total spin multiplicity of 12. Performing this calculation as described earlier, we obtain $R\leqslant 1.7$. Given that the binding energies are similar (using the method described above, we expect that production of ${}^{4}\mathrm{H}$ is suppressed by 0.79 relative to ${}^{4}_{\Lambda}\mathrm{H}$), this ratio does not necessarily indicate any extra suppression due to the coalescence of strangeness.

V. SUMMARY

We have made a measurement of the production of ${}^{3}_{\Lambda}\mathrm{H}$ and set an upper limit for the production of ${}^{4}_{\Lambda}\mathrm{H}$ in central Au-Au collisions at the AGS. Naively, the results would seem to imply an extra suppression factor for the coalescence of strangeness. However, using simple model calculations we have found that the low yields may be explained by the combined effects of the small binding energies and the large sizes of these hypernuclei. With these effects taken into account, the measured production level of the ${}^{3}_{\Lambda}\mathrm{H}$ would seem to rule out any such large penalty for strangeness coalescence. However, the low statistical significance of the signal makes it impossible to make a definitive statement from this data.

ACKNOWLEDGMENTS

We gratefully acknowledge the efforts of the AGS staff in providing the beam. This work was supported in part by grants from the Department of Energy (DOE) High Energy Physics Division, the DOE Nuclear Physics Division, and the National Science Foundation.

[1] J. Schaffner, H. Stöcker, U. Frankfurt, and C. Greiner, Phys. Rev. C **46**, 322 (1992).
[2] E. Witten, Phys. Rev. D **30**, 272 (1984).
[3] E. Farhi and R. L. Jaffe, Phys. Rev. D **30**, 2379 (1984).
[4] R. L. Jaffe, Phys. Rev. Lett. **38**, 195 (1977).
[5] T. A. Armstrong *et al.*, Phys. Rev. Lett. **79**, 3612 (1997).
[6] T. A. Armstrong *et al.*, Nucl. Phys. **A625**, 494 (1997).
[7] T. A. Armstrong *et al.*, Phys. Rev. C **63**, 054903 (2001).
[8] H. Liu and G. Shaw, Phys. Rev. D **30**, 1137 (1984).
[9] H. J. Crawford, Mukesh S. Desai, and Gordon L. Shaw, Phys. Rev. D **45**, 857 (1992).
[10] C. Greiner and J. Schaffner, preprint nucl-th/9801062.
[11] A. J. Baltz, C. B. Dover, S. H. Kahana, Y. Pang, T. J. Schlagel, and E. Schnedermann, Phys. Lett. B **325**, 7 (1994).
[12] P. Braun-Munzinger, J. Stachel, J. P. Wessels, and N. Xu, Phys. Lett. B **344**, 43 (1995).
[13] P. Braun-Munzinger and J. Stachel, J. Phys. G **21**, L17 (1995).
[14] R. Rafelski and B. Muller, Phys. Rev. Lett. **48**, 1066 (1982).
[15] R. Rafelski and B. Muller, Phys. Rev. Lett. **56**, 2334E (1986).
[16] T. A. Armstrong *et al.*, Phys. Rev. C **61**, 064908 (2000).
[17] T. A. Armstrong *et al.*, Nucl. Instrum. Methods Phys. Res. A **437**, 222 (1999).
[18] T. A. Armstrong *et al.*, Nucl. Instrum. Methods Phys. Res. A **406**, 227 (1998).
[19] T. A. Armstrong *et al.*, Nucl. Instrum. Methods Phys. Res. A **421**, 431 (1999).
[20] H. Kamada, J. Golak, K. Miyagawa, H. Witala, and W. Glöckle, Phys. Rev. C **57**, 1595 (1998).
[21] W. Glöckle, K. Miyagawa, H. Kamada, J. Golak, and H. Witala, Nucl. Phys. **A639**, 297c (1998).
[22] S. Ahmad, B. E. Bonner, S. V. Efremov, G. S. Mutchler, E. D. Platner, and H. W. Themann, Nucl. Phys. **A636**, 507 (1998).
[23] J. Barrette *et al.*, Phys. Rev. C **63**, 014902 (2001).
[24] I. Kumagai-Fuse, S. Okabe, and Y. Akaishi, Nucl. Phys. **A585**, 365c (1995).
[25] H. Outa, M. Aoki, R. S. Hayano, T. Ishikawa, M. Iwasaki, A. Sakaguchi, E. Takada, H. Tamura, and T. Yamazaki, Nucl. Phys. **A639**, 251c (1998).
[26] Particle Data Group, Phys. Rev. D **45**, III.39 (1992).
[27] R. Scheibl and U. Heinz, Phys. Rev. C **59**, 1585 (1999).
[28] Hidekatsu Nemura, Yasuyuki Suzuki, Yoshikazu Fujiwara, and Choki Nakamoto, Prog. Theor. Phys. **103**, 929 (2000).
[29] J. Barrette *et al.*, Phys. Rev. C **60**, 054905 (1999).
[30] J. Barrette *et al.*, Phys. Rev. Lett. **78**, 2916 (1997).
[31] M. Lisa *et al.*, Nucl. Phys. **A661**, 444 (1999).
[32] D. Miskowiec *et al.*, Nucl. Phys. **A610**, 227c (1996).
[33] K. Filimonov *et al.*, Nucl. Phys. **A661**, 198c (1999).
[34] T. A. Armstrong *et al.*, Phys. Rev. Lett. **83**, 5431 (1999).
[35] T. A. Armstrong *et al.*, Phys. Rev. C **65**, 014906 (2002).